Cerebral volume and diffusion MRI changes in children with sensorineural hearing loss

Peter K. Moon[a], Jason Z. Qian[b], Emily McKenna[c], Kevin Xi[c], Nathan C. Rowe[d], Nathan N. Ng[a], Jimmy Zheng[a], Lydia T. Tam[a], Sarah J. MacEachern[e], Iram Ahmad[b], Alan G. Cheng[b], Nils D. Forkert[d], Kristen W. Yeom[c],*

[a] Stanford University School of Medicine, Stanford, CA, USA
[b] Department of Otolaryngology-Head and Neck Surgery, Stanford University, Stanford, CA, USA
[c] Department of Radiology, Lucile Packard Children's Hospital, Stanford University, Stanford, CA, USA
[d] Department of Radiology, University of Calgary, Calgary, Alberta, Canada
[e] Department of Pediatrics, University of Calgary, Calgary, Alberta, Canada

ARTICLE INFO

ABSTRACT

Purpose: Sensorineural hearing loss (SNHL) is the most prevalent congenital sensory deficit in children. Information regarding underlying brain microstructure could offer insight into neural development in deaf children and potentially guide therapies that optimize language development. We sought to quantitatively evaluate MRI-based cerebral volume and gray matter microstructure children with SNHL.
Methods & Materials: We conducted a retrospective study of children with SNHL who obtained brain MRI at 3 T. The study cohort comprised 63 children with congenital SNHL without known focal brain lesion or structural abnormality (33 males; mean age 5.3 years; age range 1 to 11.8 years) and 64 age-matched controls without neurological, developmental, or MRI-based brain macrostructure abnormality. An atlas-based analysis was used to extract quantitative volume and median diffusivity (ADC) in the following brain regions: cerebral cortex, thalamus, caudate, putamen, globus pallidus, hippocampus, amygdala, nucleus accumbens, brain stem, and cerebral white matter. SNHL patients were further stratified by severity scores and hearing loss etiology.
Results: Children with SNHL showed higher median ADC of the cortex ($p = .019$), thalamus ($p < .001$), caudate ($p = .005$), and brainstem ($p = .003$) and smaller brainstem volumes ($p = .007$) compared to controls. Patients with profound bilateral SNHL did not show any significant differences compared to patients with milder bilateral SNHL, but both cohorts independently had smaller brainstem volumes compared to controls. Children with unilateral SNHL showed greater amygdala volumes compared to controls ($p = .021$), but no differences were found comparing unilateral SNHL to bilateral SNHL. Based on etiology for SNHL, patients with Pendrin mutations showed higher ADC values in the brainstem ($p = .029$, respectively); patients with Connexin 26 showed higher ADC values in both the thalamus ($p < .001$) and brainstem ($p < .001$) compared to controls.
Conclusion: SNHL patients showed significant differences in diffusion and volume in brain subregions, with region-specific findings for patients with Connexin 26 and Pendrin mutations. Future longitudinal studies could examine macro- and microstructure changes in children with SNHL over development and potential predictive role for MRI after interventions including cochlear implant outcome.

1. Introduction

Sensorineural hearing loss (SNHL) is the most prevalent congenital sensory deficit in children, affecting 6 in 1000 by age 18 (Huang et al., 2012), and occurs as a result of inner ear dysfunction caused by genetic mutation, prenatal and postnatal infection, or prematurity (Chen and Oghalai, 2016). Genetic causes have the highest prevalence, including

Pendrin and Connexin mutations (Morton and Nance, 2006); while common infectious etiologies include rubella and cytomegalovirus. SNHL is strongly associated with developmental delay (Chen and Oghalai, 2016); therefore, early detection and intervention is critical. Once hearing loss has been detected, patients often undergo imaging workup to identify etiology and also to assess for cochlear implant candidacy (Bess et al., 1998).

CT and MRI are both considered diagnostic standards for imaging workup, with each modality offering different benefits (Huang et al., 2012). MRI has quickly gained traction as a diagnostic and research tool that can evaluate both the inner ear and brain, (Kachniarz et al., 2015) and potentially uncover pre-existing brain injury or underlying congenital brain malformations that might provide insight into prognostic and developmental outcomes after cochlear implant (Weiss et al., 2012; Noij et al., 2015).

As a quantitative measure of water motion in tissue, diffusion MRI has shown utility for not only assessing brain pathology such as stroke or demyelination (Inglese and Bester, 2010), but also microstructural changes that might not be visible at the macrostructural level (Araki et al., 2015). Diffusion tensor MRI, a method that applies multiple gradient directions for image acquisition has been used to examine white matter in the auditory pathway of SNHL patients (Lin et al., 2008; Huang et al., 2015; Jiang et al., 2019; Chang et al., 2004). Studies have also interrogated cortical regions, showing altered microstructural integrity in these areas (Zheng et al., 2017; Wu et al., 2016). Wu et al. observed decreased fractional anisotropy (FA) in the superior temporal gyrus while Zheng et al. observed decreased FA and median diffusivity (ADC) in the temporal and frontal gyri, suggestive of broadly compromised myelin and axonal integrity. However, no prior study has examined gray matter (GM) diffusion properties and cerebral volume in pediatric deafness. In the context of language and learning deficits that children with SNHL often face, evaluating brain microstructure could provide insight into cortical and deep gray neural development. In this study, we sought to evaluate brain subregion volume and diffusion in children with SNHL. We hypothesized that MRI-based GM diffusion metrics are altered and might provide insight into region-specific cerebral microstructural alterations in children with SNHL.

2. Methods

2.1. Study cohort

All consecutive SNHL patients who presented for brain MRI from 2010 to 2018 at the Lucile Packard Children's Hospital at Stanford University were retrospectively reviewed after approval by the institutional review board and consent/assent waiver. The inclusion criteria were patients obtained MRI brain at 3 T with a negative MRI report; presented with history of SNHL in at least one ear as documented by audiologic studies; and patients were in pre-cochlear implant status. Exclusion criteria were corrupt imaging due to metal, hardware (e.g. dental braces), and motion.

The control group comprised 64 age-matched children with no known neurologic, neurocognitive, developmental, or behavioral deficits who had *normal-appearing* brains on MRI and without underlying sensorineural or conductive hearing loss based on detailed clinical chart review. Control subjects obtained brain MRI at 3 T as a standard of care as previously described (Forkert et al., 2016). Examples of clinical reasons for imaging were syncope, nausea, family history of aneurysm or cancers, cancer screening (e.g. P53 mutation), scalp nevus, isolated facial lesions, naso-orbital dermoid, orbital strabismus, sinus disease or inflammatory nasal obstruction, and familial short stature. Expert clinical pediatric neuroradiologist (KWY, > 10-years' experience) performed additional quality control of the MRI scans to ensure *normal-appearing* brain macrostructure of the control group.

2.2. Clinical and temporal bone data

We performed a chart review to identify hearing loss etiology, including genetic/molecular features, such as Pendrin and Connexin 26 mutations. The SNHL group was further stratified by hearing loss severity based on the pure-tone audiogram or auditory brainstem response test performed closest to the MRI date. Severity was categorized based on the frequency where the highest decibel hearing loss occurred

Table 1
Baseline characteristics of patients.

Characteristics	Normal Hearing Control Patients (N = 64)	Sensorineural Hearing Loss Patients (N = 63)
Age at Imaging (in years)[a]		
Mean ± Standard Deviation	5.8 ± 3.6	5.3 ± 3.2
Sex – no. (%)[b]		
M	29 (45.3)	33 (52.3)
F	35 (54.7)	30 (47.7)
Hearing Loss Severity – no. (%)		
Unilateral		13 (20.6)
Bilateral (profound)		28 (44.4)
Bilateral (all other severities)		22 (35.0)
Inner Ear Abnormality – no. (%)		
Enlarged Vestibular Aqueduct		5 (7.9)
Cochlear malformation		1 (1.6)
Labyrinthitis ossificans		3 (4.8)
Cochlear nerve hypoplasia/ aplasia		1 (1.6)
Multiple abnormalities		5 (7.9)
Hearing Loss Etiology – no. (%)		
Connexin 26 mutation		9 (14.2)
Pendrin mutation		8 (12.7)
Cytomegalovirus		6 (9.5)
Meningitis		1 (1.6)
Unknown		39 (62.0)
Cochlear Implant Status – no. (%)		
Recipient		25 (39.7)

[a]*T*-value = − 0.942, P-value = 0.348.
[b]χ^2-value = 0.383, P-value = 0.536.

(see Supplemental Table 1). We also consulted all available MRI/CT temporal bone studies to identify presence of inner ear abnormalities in SNHL patients (Table 1) and reviewed the clinical records for underlying cognitive dysfunction or learning disability that required interventions or individualized educational plan.

2.3. MRI method

All subjects underwent brain MRI using a single scanner at 3 T (Discovery 750 W; GE Healthcare, Milwaukee, Wisconsin) with an 8-channel head coil. Echo-planar whole-brain DWI was acquired in all cases with TR = 1500 ms, TE = 37 ms, flip angle = 90°, FOV = 24 cm^2, acceleration factor = 2, in-plane resolution = 0.94 mm^2, acquisition matrix = 128 × 128 interpolated to a 256 × 256 matrix, 44 sections with 4-mm slice thickness, no skip, 2 diffusion-weightings of $b = 0$ s/mm^2 and $b = 1000$ s/mm^2, with diffusion gradients acquired in 3 directions averaged for the latter.

2.4. Image processing

A customized image-processing pipeline was used in this work to extract quantitative values of regional brain volume and ADC values, previously described in more detail by Forkert et al (Forkert et al., 2016). In brief, after rigid registration of the DWI dataset acquired with and without diffusion-weighting for motion correction, the quantitative ADC parameter map was calculated (Stejskal and Tanner, 1965). For regional diffusion and volumetric analysis, the Montreal Neurological Institute-152 brain atlas was registered to the DWI dataset using a non-linear transformation, which was then used to warp the Harvard-Oxford subcortical atlas brain regions to the subject-specific brain anatomy (Mazziotta et al., 2001). Brain regions included in this brain atlas are the cerebral cortex, cerebral WM, thalamus, caudate, putamen, globus pallidus, amygdala, hippocampus, brain stem, and nucleus accumbens. Two experienced observers (KWY, > 10-years experience; NDF, > 10-

years experience) checked all registration results and patients with insufficient or suboptimal registration results were excluded from further analyses. The aligned brain atlas regions were then used to measure the corresponding regional brain volumes and median ADC values combined for corresponding brain structures in the left and right hemispheres. The lateral ventricles were only used for volumetric assessment.

2.5. Statistical analysis

MANCOVA was used in three separate analyses for group comparison using the volumetric and median ADC values as dependent variables, age at imaging and sex as covariates. Class was a fixed factor but differed in each analysis. In the first analysis, class was defined by two groups: control (no hearing loss) and all subjects with SNHL. In the second analysis, class was defined by three groups: control; profound bilateral SNHL; other bilateral SNHL (patients who did not meet criteria for profound bilateral SNHL). In the third analysis, class was defined by three groups: control; unilateral SNHL; bilateral SNHL. SPSS (Version 24.0, IBM, Armonk, NY) was used for MANCOVA statistical analyses. In the fourth analysis, a series of univariate analyses was conducted comparing each etiology to control, due to the small number per etiology. A P value < 0.05 (Bonferroni-corrected) was considered significant. We corrected for age as a covariate without additional age-matching in the second, third, and fourth analyses due to the limited number of patients.

For the second and third MANCOVA analyses, post hoc pair-wise analyses were performed to generate the estimated marginal means, confidence intervals, and p-values required for plotting (Figs. 1, 2). The plots were generated using the R statistical software package of The R Foundation of Statistical Computing (Version 3.2.2; www.r-project. org).

3. Results

3.1. Clinical characteristics

63 SNHL patients [33 males; mean age 5.3 years; range 1 to 11.8 years; standard deviation 3.2 years], who met the inclusion criteria and passed the image quality control for the study, were compared against 64 age-matched controls (29 males; mean age 5.8 years; standard deviation 3.6 years) (Table 1).

Of the 63 SNHL patients, 13 patients had unilateral SNHL and 50 bilateral SNHL (B-SNHL). Audiologic studies were conducted on average 1.0 months prior to MRI (standard deviation 22.7 months). Among those with B-SNHL, 28 patients had profound B-SNHL (Profound B-SNHL) and 22 patients had milder forms of B-SNHL (Other B-SNHL). Etiologies for SNHL were: Connexin 26 mutation (n = 9), Pendrin mutations (n = 8), history of cytomegalovirus infection (n = 6), and meningitis (n = 1). Etiology was unknown for 39 individuals. Fifteen patients showed inner ear abnormalities based on either MRI or CT temporal bone assessment, summarized in Table 1. 25 patients eventually received cochlear implant. Based on available clinical records, information regarding language development, school performance, or other developmental features are shown in Supplemental Table 2.

3.2. Diffusion MRI and volume analysis

Comparison of the entire SNHL cohort and controls showed statistically significant differences in median ADC of brain subregions (p < .001). Post hoc pair-wise analysis comparing SNHL cohort to controls revealed significantly increased median ADC values for the cerebral cortex, thalamus, caudate, and brainstem, as well as decrease in brainstem volume (Table 2). Graphs of the estimated marginal means and 95% confidence intervals generated by post hoc pair-wise analysis are shown in Fig. 1.

Fig. 1. Volume and Apparent Diffusion Coefficient graphs comparing estimated marginal means and 95% confidence intervals of the following factors from the 1st MANCOVA: control (N), Hearing Loss (HL). p-values and significance generated from post hoc pair-wise analysis are denoted as follows: N.S. p > .10, * p < .05, ** p < .01, *** p < .001 (Bonferroni-corrected).
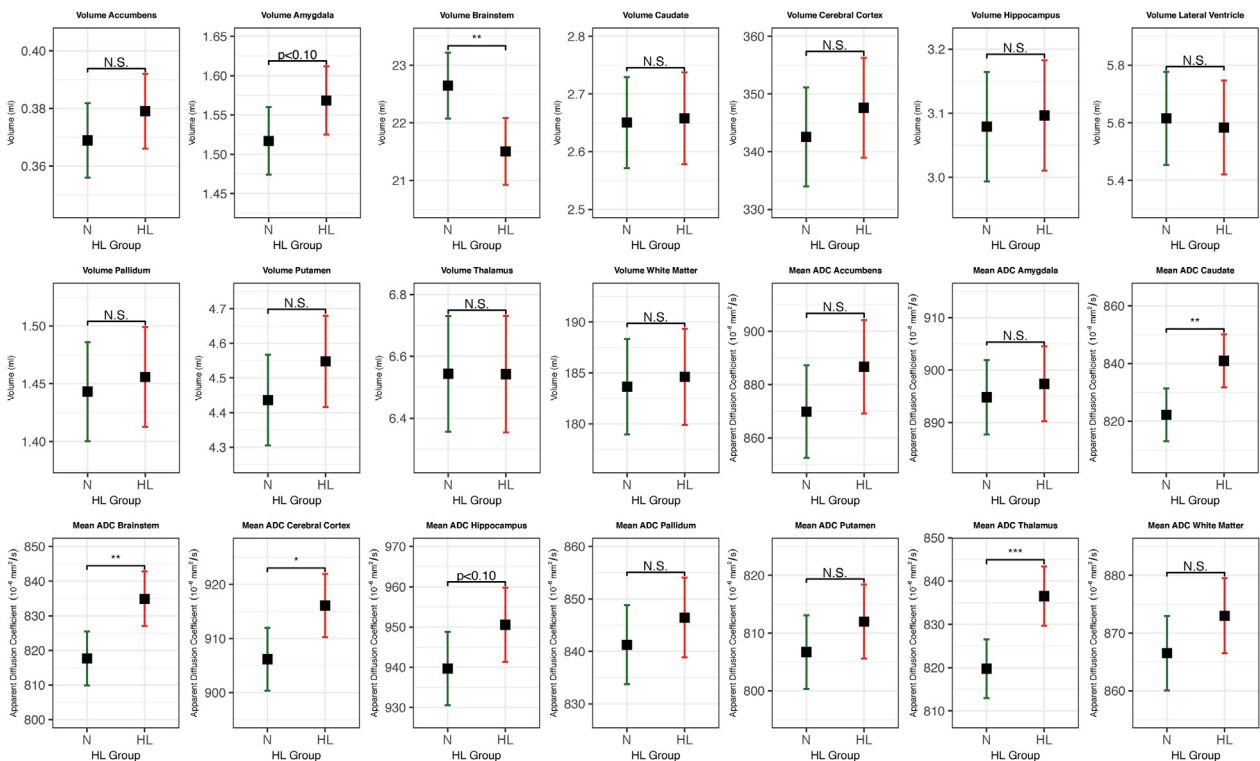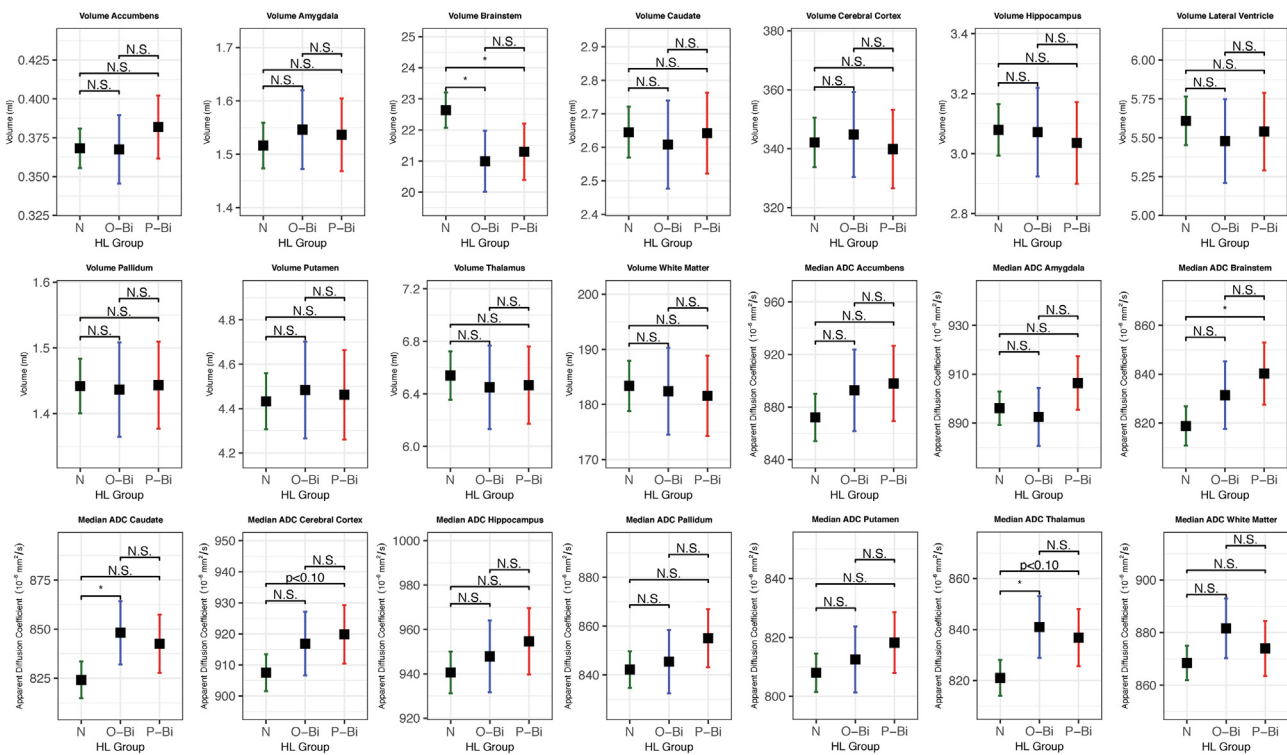
Fig. 2. Volume and Apparent Diffusion Coefficient graphs comparing estimated marginal means and 95% confidence intervals of the following factors from the 2nd MANCOVA: control (N), other bilateral hearing loss (O-Bi), profound bilateral hearing loss (P-Bi). p-values and significance generated from post hoc pair-wise analysis are denoted as follows: N.S. p > .10, * p < .05, ** p < .01, *** p < .001 (Bonferroni-corrected).

The second analysis also showed some differences between Profound B-SNHL, Other B-SNHL, and controls (p < .001). Compared to controls, the Profound B-SNHL cohort had higher median ADC values in the brainstem, whereas the Other B-SNHL group showed higher median ADC in the thalamus and caudate. Additionally, the brainstem volume in both the Profound B-SNHL and Other B-SNHL groups was

significantly smaller than controls (Table 3). Comparison between Profound B-SNHL and Other B-SNHL groups showed no significant difference in either median ADC values or volumes. Graphs of the second pair-wise analysis are shown in Fig. 2.

In the third analysis, the U-SNHL cohort showed greater amygdala volumes compared to controls (Table 4). The B-SNHL cohort

Table 2
Volumetric, apparent diffusion coefficient values analyses by brain region after 1st MANCOVA. Factors: Control (N), SNHL.

	Control (N = 64)				SNHL (N = 63)				Univariate Test	
	Mean[a]	SE	Lower95% CI	Upper 95% CI	Mean[a]	SE	Lower 95% CI	Upper 95% CI	Mean Diff.	p-value[b]
Volume (mL)										
Cerebral white matter	183.6	2.37	178.9	188.3	184.6	2.39	179.9	189.3	0.98	0.773
Cerebral cortex	342.6	4.34	334.0	351.2	347.6	4.38	339.0	356.3	5.05	0.416
Lateral ventricle	5.62	0.08	5.45	5.78	5.58	0.08	5.42	5.75	−0.03	0.785
Thalamus	6.54	0.09	6.36	6.73	6.54	0.10	6.35	6.73	0.00	0.993
Caudate	2.65	0.04	2.57	2.73	2.66	0.04	2.58	2.74	0.01	0.896
Putamen	4.44	0.07	4.31	4.57	4.55	0.07	4.42	4.68	0.11	0.236
Pallidum	1.44	0.02	1.40	1.49	1.46	0.02	1.41	1.50	0.01	0.683
Hippocampus	3.08	0.04	2.99	3.16	3.10	0.04	3.01	3.18	0.02	0.777
Amygdala	1.52	0.02	1.47	1.56	1.57	0.02	1.53	1.61	0.05	0.099
Accumbens	0.37	0.01	0.36	0.38	0.38	0.01	0.37	0.39	0.01	0.276
Brainstem	22.65	0.29	22.07	23.22	21.51	0.29	20.93	22.08	−1.14	**0.007[c]**
Median ADC (10^{-6} mm²/s)										
Cerebral white matter	866.5	3.26	860.1	873.0	873.0	3.29	866.5	879.5	6.49	0.165
Cerebral cortex	906.2	2.93	900.4	912.0	916.1	2.95	910.2	921.9	9.91	**0.019[c]**
Thalamus	819.8	3.43	813.0	826.5	836.5	3.46	829.7	843.4	16.78	**< 0.001[c]**
Caudate	822.3	4.62	813.1	831.4	840.9	4.65	831.7	850.1	18.67	**0.005[c]**
Putamen	806.7	3.23	800.3	813.1	812.0	3.25	805.6	818.4	5.29	0.251
Pallidum	841.3	3.81	833.7	848.8	846.5	3.84	838.8	854.1	5.19	0.341
Hippocampus	939.6	4.61	930.5	948.8	950.6	4.65	941.3	959.8	10.91	0.100
Amygdala	894.8	3.58	887.7	901.9	897.4	3.61	890.2	904.5	2.55	0.619
Accumbens	869.9	8.79	852.5	887.3	886.7	8.86	869.1	904.2	16.83	0.181
Brainstem	817.7	3.95	809.8	825.5	834.9	3.98	827.0	842.8	17.22	**0.003[c]**

[a]Covariates appearing in the model are evaluated at the following values: age (months) at time of MRI = 66.65, sex = 0.51.
[b]Based on the linearly independent pairwise comparisons among the estimated marginal means.
[c]P < 0.05 for statistical significance, Bonferroni-corrected.

Table 3
Volumetric, apparent diffusion coefficient values analyses by brain region after 2nd MANCOVA. Factors: Control, Other Profound B-SNHL, Other B-SNHL.

	Control (N = 64)		Other B-SNHL (N = 22)		Profound B-SNHL (N = 28)		Univariate Test					
	Mean[a]	SE	Mean[a]	SE	Mean[a]	SE	Mean Diff.[c]	p-value[b]	Mean Diff.[d]	p-value[b]	Mean Diff.[e]	p-value[b]
Volume (mL)												
Cerebral white matter	183.4	2.31	182.4	3.98	181.6	3.67	0.98	1.000	1.80	1.000	0.82	1.000
Cerebral cortex	342.1	4.23	344.8	7.29	339.9	6.72	−2.70	1.000	2.26	1.000	4.96	1.000
Lateral ventricle	5.61	0.08	5.48	0.14	5.54	0.13	0.13	1.000	0.07	1.000	−0.06	1.000
Thalamus	6.54	0.09	6.45	0.16	6.47	0.15	0.09	1.000	0.07	1.000	−0.02	1.000
Caudate	2.65	0.04	2.61	0.07	2.64	0.06	0.04	1.000	0.00	1.000	−0.03	1.000
Putamen	4.43	0.06	4.48	0.11	4.46	0.10	−0.05	1.000	−0.03	1.000	0.02	1.000
Pallidum	1.44	0.02	1.44	0.04	1.44	0.03	0.01	1.000	0.00	1.000	−0.01	1.000
Hippocampus	3.08	0.04	3.07	0.07	3.04	0.07	0.01	1.000	0.04	1.000	0.04	1.000
Amygdala	1.52	0.02	1.54	0.04	1.54	0.03	−0.03	1.000	−0.02	1.000	0.01	1.000
Accumbens	0.37	0.01	0.37	0.01	0.38	0.01	0.00	1.000	−0.01	0.809	−0.01	1.000
Brainstem	22.64	0.29	21.00	0.50	21.30	0.46	1.64	**0.014[f]**	1.34	**0.050[f]**	−0.30	1.000
Median ADC (10^{-6} mm^2/s)												
Cerebral white matter	868.4	3.31	881.6	6.71	873.9	5.26	−13.16	0.140	−5.51	1.000	7.65	1.000
Cerebral cortex	907.5	2.99	916.9	5.16	919.8	4.76	−9.35	0.350	−12.34	0.100	−2.98	1.000
Thalamus	821.0	3.55	840.9	6.13	836.8	5.65	−19.92	**0.016[f]**	−15.81	0.066	4.11	1.000
Caudate	824.2	4.72	848.2	8.15	842.6	7.51	−24.01	**0.034[f]**	−18.44	0.131	5.58	1.000
Putamen	808.0	3.29	812.5	5.67	818.2	5.23	−4.52	1.000	−10.24	0.320	−5.72	1.000
Pallidum	842.2	3.79	845.4	6.53	855.0	6.02	−3.23	1.000	−12.80	0.240	−9.57	0.895
Hippocampus	940.6	4.75	947.8	8.19	954.6	7.55	−7.23	1.000	−14.04	0.375	−6.81	1.000
Amygdala	896.1	3.48	892.5	6.00	906.3	5.53	3.90	1.000	−10.26	0.377	−13.86	0.306
Accumbens	872.1	9.09	892.7	15.69	897.9	14.46	−20.65	0.760	−25.86	0.420	−5.21	1.000
Brainstem	818.8	4.05	831.4	6.98	840.2	6.44	−12.61	0.353	−21.45	**0.020[f]**	−8.84	1.000

[a]Covariates appearing in the model are evaluated at the following values: age (months) at time of MRI = 64.86, sex = 0.49.
[b]Based on the linearly independent pairwise comparisons among the estimated marginal means.
[c]Control – Other Bilateral.
[d]Control – Profound Bilateral.
[e]Other Bilateral – Profound Bilateral.
[f]P < 0.05 for statistical significance, Bonferroni-corrected.

Table 4
Volumetric, apparent diffusion coefficient values analyses by brain region after 3rd MANCOVA. Factors: Control, Bilateral, Unilateral.

	Control (N = 64)		Bilateral (N = 50)		Unilateral (N = 13)		Univariate Test					
	Mean[a]	SE	Mean[a]	SE	Mean[a]	SE	Mean Diff.[c]	p-value[b]	Mean Diff.[d]	p-value[b]	Mean Diff.[e]	p-value[b]
Volume (mL)												
Cerebral white matter	183.7	2.34	182.1	2.68	193.7	5.26	1.57	1.000	−10.02	0.249	−11.59	0.164
Cerebral cortex	342.7	4.28	342.5	4.89	366.4	9.59	0.19	1.000	−23.65	0.076	−23.84	0.091
Lateral ventricle	5.62	0.08	5.52	0.09	5.83	0.18	0.10	1.000	−0.21	0.879	−0.31	0.412
Thalamus	6.55	0.09	6.46	0.11	6.84	0.21	0.08	1.000	−0.29	0.619	−0.38	0.358
Caudate	2.65	0.04	2.63	0.05	2.76	0.09	0.02	1.000	−0.11	0.779	−0.13	0.590
Putamen	4.44	0.07	4.48	0.07	4.81	0.15	−0.04	1.000	−0.37	0.064	−0.33	0.142
Pallidum	1.44	0.02	1.44	0.02	1.51	0.05	0.00	1.000	−0.07	0.661	−0.07	0.673
Hippocampus	3.08	0.04	3.06	0.05	3.24	0.10	0.02	1.000	−0.16	0.357	−0.19	0.260
Amygdala	1.52	0.02	1.54	0.02	1.66	0.05	−0.03	1.000	−0.14	**0.021[f]**	−0.12	0.098
Accumbens	0.37	0.01	0.38	0.01	0.39	0.01	0.00	1.000	−0.02	0.422	−0.02	0.901
Brainstem	22.66	0.29	21.19	0.33	22.66	0.64	1.46	**0.033[f]**	0.00	1.000	−1.47	0.140
Median ADC (10^{-6} mm^2/s)												
Cerebral white matter	866.4	3.34	876.0	3.71	861.9	7.26	−9.59	0.165	4.53	1.000	14.11	0.268
Cerebral cortex	906.1	2.93	917.5	3.36	910.9	6.58	−11.37	**0.038[f]**	−4.75	1.000	6.62	1.000
Thalamus	819.7	3.44	837.9	3.94	831.5	7.71	−18.20	**0.002[f]**	−11.77	0.492	6.43	1.000
Caudate	822.2	4.61	843.9	5.28	829.7	10.34	−21.79	**0.007[f]**	−7.58	1.000	14.21	0.685
Putamen	806.6	3.21	814.6	3.67	802.4	7.20	−7.97	0.321	4.21	1.000	12.19	0.416
Pallidum	841.2	3.79	849.8	4.34	834.1	8.50	−8.64	0.416	7.04	1.000	15.68	0.320
Hippocampus	939.6	4.63	950.7	5.30	949.9	10.39	−11.09	0.361	−10.25	1.000	0.84	1.000
Amygdala	894.8	3.59	898.9	4.11	891.8	8.05	−4.09	1.000	2.95	1.000	7.04	1.000
Accumbens	869.6	8.75	893.9	10.01	859.9	19.62	−24.30	0.215	9.70	1.000	34.00	0.388
Brainstem	817.7	3.97	835.3	4.54	833.3	8.90	−17.65	**0.013[f]**	−15.69	0.325	1.96	1.000

[a]Covariates appearing in the model are evaluated at the following values: age (months) at time of MRI = 66.65, sex = 0.51.
[b]Based on the linearly independent pairwise comparisons among the estimated marginal means.
[c]Control – Bilateral.
[d]Control – Unilateral.
[e]Bilateral – Unilateral.
[f]P < 0.05 for statistical significance, Bonferroni-corrected.
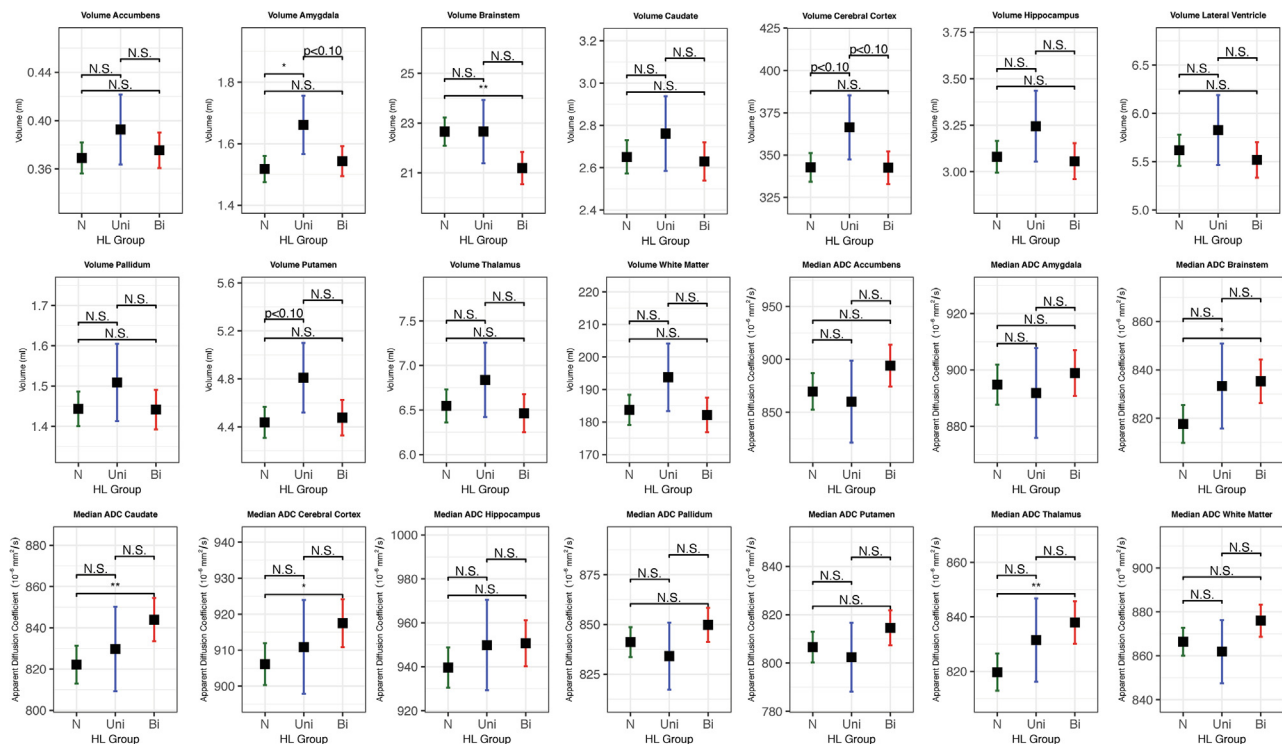
Fig. 3. Volume and Apparent Diffusion Coefficient graphs comparing estimated marginal means and 95% confidence intervals of the following factors from the 3rd MANCOVA: control (N), unilateral hearing loss (Uni), bilateral hearing loss (Bi). p-values and significance generated from post hoc pair-wise analysis are denoted as follows: N.S. $p > .10$, * $p < .05$, ** $p < .01$, *** $p < .001$ (Bonferroni-corrected).

maintained the same significant trends as the entire SNHL cohort when compared controls. Finally, comparison between U-SNHL to B-SNHL groups showed no significant difference in either median ADC values or volumes. Graphs from the third pair-wise analysis are shown in Fig. 3.

Based on etiology for SNHL, patients with Connexin 26 mutations had significantly higher ADC values in the thalamus ($p < .001$) and brainstem ($p < .001$). Patients with Pendrin mutations also had higher ADC values in the brainstem ($p = .029$) with a trend of increased ADC values in the thalamus ($p = .067$). (Fig. 4). 44 percent of patients with Connexin 26 mutations and 75 percent of patients with Pendrin mutations had Profound B-SNHL (range for all etiologies: 0 to 75 percent). No other etiology showed significant differences compared to controls.

After correcting for age as a covariate for the second, third, and fourth analyses due to the limited number of patients, we found the following. There were no differences in sex between the groups in the second analysis ($p = 0.25$), no differences in age ($p = 0.11$) or sex ($p = 0.16$) between groups in the third analysis, and no differences in age (Connexin 26, $p = 0.87$; Pendrin, $p = 0.95$) or sex (Connexin 26, $p = 0.34$; Pendrin, $p = 1.00$) by etiology. However, the second analysis showed differences in age ($p < 0.001$).

4. Discussion

We found significant differences in brain subregion mean diffusivity and volume in children with SNHL, with decreases in brainstem volumes of both Profound B-SNHL and Other SNHL compared to controls. No differences were found comparing Profound B-SNHL to Other SNHL, or unilateral SNHL to bilateral SNHL. However, children with unilateral SNHL showed greater amygdala volumes compared to controls. Among different etiologies for SNHL, patients with a Connexin 26 or Pendrin mutations exhibited abnormal diffusion of the thalamus and brainstem. We aimed at evaluating microstructural properties of the cerebral GM given the strong association between congenital hearing loss, cognitive dysfunction, and developmental delay in children with SNHL (Bess et al., 1998; Stika et al., 2015; Psarommatis et al., 2001). We used

diffusion MRI, which has shown high reproducibility and is often acquired as part of standard brain and temporal bone MRI (Grech-Sollars et al., 2015) to interrogate specific GM regions of the brain, previously unexplored in deaf children. We also evaluated regional cerebral volume given general lack of brain volumetric data in pediatric deafness.

Multiple factors likely contributed to altered diffusion of the cerebral cortex given a well-established link between hearing and language function. For example, studies have shown that hearing loss adversely affects receptive and expressive language development (Yoshinaga-Itano et al., 1998; Moeller, 2000). Broca's area, Wernicke's area and the angular gyrus are specialized centers for language, all located in the cerebral cortex. Prefrontal cortex functions as the center for working memory, and has also been shown impacted in children with hearing loss (Hansson et al., 2004; Rudner and Holmer, 2016). A large number of our hearing loss patients also required individualized education plans or language therapies (see Supplemental Table 2). Alteration of diffusion may also reflect re-structuring of cortical connectivity or functionality from cross-modal plasticity, i.e. re-allocation of cortical resources to compensate for sensory deficits (Sharma and Glick, 2016; Dewey and Hartley, 2015; Sharma et al., 2015). It is possible genetic mutation, teratogens, or other exogenous factors that have disrupted inner ear ontogenesis also directly *or* indirectly contributed to altered cortical microstructure.

Across all SNHL groups, we also found increased mean diffusivity of the brainstem and thalamus and reduced brainstem volume. Nuclei in both thalami and brainstem are known to relay sensory information to the auditory cortex. Prior studies of SNHL patients have shown abnormal WM DTI in the auditory pathway, including lateral lemniscus in the inferior colliculus (Lin et al., 2008; Huang et al., 2015; Rachakonda et al., 2014). Another study of 13 congenitally deaf patients showed DTI abnormality of the thalamo-cortical tracts (Lyness et al., 2014) and suggested this may reflect a functional sequela of auditory deprivation in deaf patients given the thalamic role in multimodal perception through cortico-thalamo-cortical connections (Jones, 2009). Our results complement prior studies and show altered GM microstructure
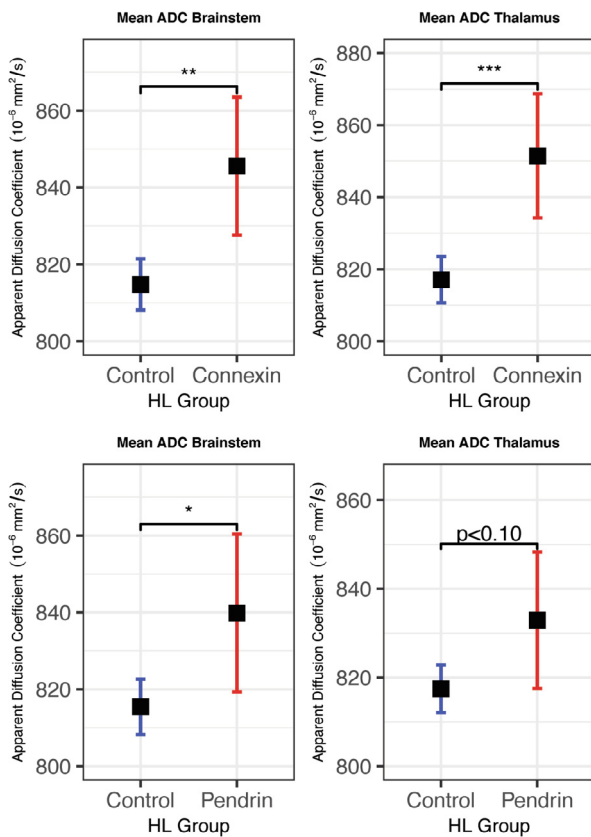
Fig. 4. Apparent Diffusion Coefficient graphs comparing estimated marginal means and 95% confidence intervals of the following factors: control; Connexin 26 or Pendrin. p-values and significance generated from post hoc pair-wise analysis are denoted as follows: N.S. p > .10, * p < .05, ** p < .01, *** p < .001 (Bonferroni-corrected).

implicated in the auditory pathway.

Microstructural alteration is expected to precede any change in macrostructure, and thus might explain altered diffusion in several cerebral GM regions (e.g. cerebral cortex, thalamus, caudate, hippocampus) without associated volume loss. Interestingly, we observed reduced volume only in the brainstem across all SNHL patients, suggesting a more chronic process. This might reflect the dependence of the brainstem development on peripheral activity originating from the cochlea or early dysfunction in connectivity between the inner ear and brainstem that precede interactions with the supratentorial brain structures (Graham and Shimeld, 2013). Atrophy of brain regions other than the brainstem (i.e. auditory cortex) has been reported in deaf adults (Lin et al., 2014; Peelle et al., 2011; Hribar et al., 2014), which suggests that over time, other brain regions, including the cortex, can suffer volume loss.

We also observed altered mean diffusivity in the caudate and an altered trend in the hippocampus (p < 0.10). Although the relationship between hearing loss and caudate and/or hippocampus is relatively unexplored, given the close relationship between memory and hearing (Hansson et al., 2004; Rönnberg et al., 2014), our findings may reflect altered connectivity in hearing loss and memory processing. Specifically, the caudate serves as the center for habit learning while the hippocampus is responsible for declarative memory. The two memory systems work in an integrated fashion to streamline multiple facets of memory processing and learning (Voermans et al., 2004; Nyberg et al., 2016; Schiffer et al., 2012). Altered microstructure of these regions may underlie learning difficulties and reduced academic achievement in children with SNHL (Ching et al., 2013; Gilani et al., 2017; Sarant et al., 2015).

Despite altered diffusion properties of the GM in several brain regions, the global WM did not show altered diffusion. Based on prior reports of abnormal tensor in the auditory pathway (Lin et al., 2008; Huang et al., 2015; Jiang et al., 2019), abnormal WM microstructure may be localized to or more pronounced in the auditory regions rather than the global WM. Since prior studies have largely focused on adult population (Lin et al., 2008; Huang et al., 2015; Jiang et al., 2019), it is also possible WM is not significantly altered in the immature or developing pediatric brain that is actively undergoing myelination, and its future status dependent on underlying genetics, auditory and language stimulation, learning environment, and therapeutic interventions.

While we did not observe any differences between U-SNHL and B-SNHL cohorts, amygdala volume was higher in the U-SNHL group compared to controls. Although significance of this finding is unclear, it may relate to its extensive connection to the insular cortex (Ghaziri et al., 2018; Ture et al., 1999). The insular cortex has been shown to reorganize in the context of unilateral hearing loss and therefore considered critical for integration and high-level auditory processing (Wang et al., 2014). Prior fMRI studies have also suggested that the amygdala has a unique role in valent sound (Booth et al., 2007; Husain et al., 2014).

Finally, we observed altered diffusion in the brainstem and thalamus of patients with Connexin 26 mutations, and the brainstem in patients with Pendrin mutations (Pendrin thalamus ADC, p = .067). Statistical significance was reached likely due to larger sample size and more homogeneous nature of the Connexin 26 and Pendrin groups compared to other etiologies. Regardless, our results prompt future larger, etiology-specific MRI studies that investigate neural development or biomarkers of prognosis in SNHL patients.

There are several limitations to this study. As a retrospective study, we performed a cross-sectional investigation and did not examine longitudinal brain developmental changes. Given that a large majority of our patients had profound SNHL, determining the relationship between milder forms or asymmetric/ unilateral hearing impairment was limited. We corrected for age as a covariate for the second, third, and fourth analyses without prior age-matching due to the limited number of patients, but findings based on a limited number of patients should be interpreted with caution. We combined data from both hemispheres to reduce the number of hypotheses tested, which omitted trends in laterality. We also recognize that registration of small brain regions could render imprecise segmentation, but this automated procedure was conducted over both SNHL and control groups in order to reduce observer bias and a rigorous quality control was performed. There is a minor chance distortion effects could bias brainstem volume calculation. However, due to the usage of a non-linear registration, this should not affect the measured ADC values. Finally, given heterogeneous etiologies for SNHL in our cohort, direct contribution of SNHL to altered brain microstructure versus acquired, genetic, or molecular events that contributed to both SNHL and alteration in brain microstructure may be difficult to distinguish.

5. Conclusion

SNHL patients showed significant brain subregion differences in diffusion and volume, particularly those with profound bilateral SNHL. Among different etiologies for SNHL, Connexin 26 and Pendrin mutations were associated with microstructural changes in the thalamus and the brainstem. This study identifies a potential clinical role for MRI in evaluating cerebral microstructure in children with SNHL. Future studies could examine roles for MRI in children with SNHL as a biomarker for language development, microstructural neural developmental changes following interventions, and its potential predictive role for cochlear implant outcome. Atlas applications such as Talairach with Brodmann approximations may also provide additional insight into microstructural changes specific to the speech and language centers in children with SNHL.

6. Disclosures

Some of the content of this manuscript has been accepted for presentation at the 2020 American Society of Pediatric Neuroradiology.

CRediT authorship contribution statement

Peter K. Moon: Formal analysis, Investigation, Writing - original draft, Visualization. **Jason Z. Qian:** Funding acquisition, Data curation, Writing - original draft. **Emily McKenna:** Data curation, Investigation. **Kevin Xi:** Data curation, Investigation. **Nathan C. Rowe:** Data curation, Validation. **Nathan N. Ng:** Formal analysis, Validation. **Jimmy Zheng:** Visualization, Formal analysis. **Lydia T. Tam:** Writing - review & editing, Investigation. **Sarah J. MacEachern:** Writing - review & editing, Investigation. **Iram Ahmad:** Data curation, Writing - review & editing. **Alan G. Cheng:** Conceptualization, Investigation, Writing - review & editing. **Nils D. Forkert:** Conceptualization, Methodology, Software, Validation, Writing - review & editing. **Kristen W. Yeom:** Conceptualization, Methodology, Writing - original draft, Supervision, Project administration.

Declaration of Competing Interest

The authors report no conflicts of interest.

Acknowledgements

References

Huang, B.Y., Zdanski, C., Castillo, M., 2012. Pediatric sensorineural hearing loss, part 2: syndromic and acquired causes. AJNR Am. J. Neuroradiol. 33 (3), 399–406. https://doi.org/10.3174/ajnr.A2499.

Chen, M.M., Oghalai, J.S., 2016. Diagnosis and management of congenital sensorineural hearing loss. Curr. Treat Options Pediatr. 2 (3), 256–265. https://doi.org/10.1007/s40746-016-0056-6.

Morton, C.C., Nance, W.E., 2006. Newborn hearing screening–a silent revolution. N. Engl. J. Med. 354 (20), 2151–2164. https://doi.org/10.1056/NEJMra050700.

Bess, F.H., Dodd-Murphy, J., Parker, R.A., 1998. Children with minimal sensorineural hearing loss: prevalence, educational performance, and functional status. Ear Hear. 19 (5), 339–354. https://doi.org/10.1097/00003446-199810000-00001.

Huang, B.Y., Zdanski, C., Castillo, M., 2012. Pediatric sensorineural hearing loss, part 1: practical aspects for neuroradiologists. AJNR Am. J. Neuroradiol. 33 (2), 211–217. https://doi.org/10.3174/ajnr.A2498.

Kachniarz, B., Chen, J.X., Gilani, S., Shin, J.J., 2015. Diagnostic yield of MRI for pediatric hearing loss: a systematic review. Otolaryngol. Head Neck Surg. 152 (1), 5–22. https://doi.org/10.1177/0194599814555837.

Weiss, J.P., Bernal, B., Balkany, T.J., Altman, N., Jethanamest, D., Andersson, E., 2012. fMRI evaluation of cochlear implant candidacy in diffuse cortical cytomegalovirus disease. Laryngoscope 122 (9), 2064–2066. https://doi.org/10.1002/lary.23243.

Noij, K.S., Remenschneider, A.K., Kozin, E.D., et al., 2015. Direct parasagittal magnetic resonance imaging of the internal auditory canal to determine cochlear or auditory brainstem implant candidacy in children. Laryngoscope 125 (10), 2382–2385. https://doi.org/10.1002/lary.25228.

Inglese, M., Bester, M., 2010. Diffusion imaging in multiple sclerosis: research and clinical implications. NMR Biomed. 23 (7), 865–872. https://doi.org/10.1002/nbm.1515.

Araki, Y., Takagi, Y., Fushimi, Y., et al., 2015. Apparent diffusion coefficient and transient neurological deficit after revascularization surgery in Moyamoya disease. J. Stroke Cerebrovasc. Dis. 24 (9), 2054–2059. https://doi.org/10.1016/j.jstrokecerebrovasdis.2015.04.026.

Lin, Y., Wang, J., Wu, C., Wai, Y., Yu, J., Ng, S., 2008. Diffusion tensor imaging of the auditory pathway in sensorineural hearing loss: changes in radial diffusivity and diffusion anisotropy. J. Magn. Reson. Imaging 28 (3), 598–603. https://doi.org/10.1002/jmri.21464.

Huang, L., Zheng, W., Wu, C., et al., 2015. Diffusion tensor imaging of the auditory neural pathway for clinical outcome of cochlear implantation in pediatric congenital sensorineural hearing loss patients. PLoS ONE 10 (10), e0140643. https://doi.org/10.1371/journal.pone.0140643.

Jiang, M., Wen, Z., Long, L., et al., 2019. Assessing cerebral white matter microstructure in children with congenital sensorineural hearing loss: a tract-based spatial statistics study. Front. Neurosci. 13, 597. https://doi.org/10.3389/fnins.2019.00597.

Chang, Y., Lee, S.-H., Lee, Y.-J., et al., 2004. Auditory neural pathway evaluation on sensorineural hearing loss using diffusion tensor imaging. NeuroReport 15 (11), 1699–1703. https://doi.org/10.1097/01.wnr.0000134584.10207.1a.

Zheng, W., Wu, C., Huang, L., Wu, R., 2017. Diffusion kurtosis imaging of microstructural alterations in the brains of paediatric patients with congenital sensorineural hearing loss. Sci. Rep. 7 (1), 1543. https://doi.org/10.1038/s41598-017-01263-9.

Wu, C., Huang, L., Tan, H., et al., 2016. Diffusion tensor imaging and MR spectroscopy of microstructural alterations and metabolite concentration changes in the auditory neural pathway of pediatric congenital sensorineural hearing loss patients. Brain Res. 1639, 228–234. https://doi.org/10.1016/j.brainres.2014.12.025.

Forkert, N.D., Li, M.D., Lober, R.M., Yeom, K.W., 2016. Gray matter growth is accompanied by increasing blood flow and decreasing apparent diffusion coefficient during childhood. AJNR Am. J. Neuroradiol. 37 (9), 1738–1744. https://doi.org/10.3174/ajnr.A4772.

Stejskal, E.O., Tanner, J.E., 1965. Spin diffusion measurements: spin echoes in the presence of a time-dependent field gradient. J. Chem. Phys. 42 (1), 288–292. https://doi.org/10.1063/1.1695690.

Mazziotta, J., Toga, A., Evans, A., et al., 2001. A probabilistic atlas and reference system for the human brain: International Consortium for Brain Mapping (ICBM). Philos. Trans. R. Soc. Lond. B Biol. Sci. 356 (1412), 1293–1322. https://doi.org/10.1098/rstb.2001.0915.

Stika, C.J., Eisenberg, L.S., Johnson, K.C., et al., 2015. Developmental outcomes of early-identified children who are hard of hearing at 12 to 18 months of age. Early Hum. Dev. 91 (1), 47–55. https://doi.org/10.1016/j.earlhumdev.2014.11.005.

Psarommatis, I.M., Goritsa, E., Douniadakis, D., Tsakanikos, M., Kontrogianni, A.D., Apostolopoulos, N., 2001. Hearing loss in speech-language delayed children. Int. J. Pediatr. Otorhinolaryngol. 58 (3), 205–210. https://doi.org/10.1016/s0165-5876(01)00430-x.

Grech-Sollars, M., Hales, P.W., Miyazaki, K., et al., 2015. Multi-centre reproducibility of diffusion MRI parameters for clinical sequences in the brain. NMR Biomed. 28 (4), 468–485. https://doi.org/10.1002/nbm.3269.

Yoshinaga-Itano, C., Sedey, A.L., Coulter, D.K., Mehl, A.L., 1998. Language of early- and later-identified children with hearing loss. Pediatrics 102 (5), 1161–1171. https://doi.org/10.1542/peds.102.5.1161.

Moeller, M.P., 2000. Early intervention and language development in children who are deaf and hard of hearing. Pediatrics 106 (3), E43. https://doi.org/10.1542/peds.106.3.e43.

Hansson, K., Forsberg, J., Lofqvist, A., Maki-Torkko, E., Sahlen, B., 2004. Working memory and novel word learning in children with hearing impairment and children with specific language impairment. Int. J. Lang. Commun. Disord. 39 (3), 401–422. https://doi.org/10.1080/13682820410001669887.

Rudner, M., Holmer, E., 2016. Working memory in deaf children is explained by the developmental ease of language understanding (D-ELU) model. Front. Psychol. 7, 1047. https://doi.org/10.3389/fpsyg.2016.01047.

Sharma, A., Glick, H., 2016. Cross-modal re-organization in clinical populations with hearing loss. Brain Sci. 6 (1). https://doi.org/10.3390/brainsci6010004.

Dewey, R.S., Hartley, D.E.H., 2015. Cortical cross-modal plasticity following deafness measured using functional near-infrared spectroscopy. Hear. Res. 325, 55–63. https://doi.org/10.1016/j.heares.2015.03.007.

Sharma, A., Campbell, J., Cardon, G., 2015. Developmental and cross-modal plasticity in deafness: evidence from the P1 and N1 event related potentials in cochlear implanted children. Int. J. Psychophysiol. 95 (2), 135–144. https://doi.org/10.1016/j.ijpsycho.2014.04.007.

Rachakonda, T., Shimony, J.S., Coalson, R.S., Lieu, J.E.C., 2014. Diffusion tensor imaging in children with unilateral hearing loss: a pilot study. Front. Syst. Neurosci. 8, 87. https://doi.org/10.3389/fnsys.2014.00087.

Lyness, R.C., Alvarez, I., Sereno, M.I., MacSweeney, M., 2014. Microstructural differences in the thalamus and thalamic radiations in the congenitally deaf. Neuroimage 100, 347–357. https://doi.org/10.1016/j.neuroimage.2014.05.077.

Jones, E.G., 2009. Synchrony in the interconnected circuitry of the thalamus and cerebral cortex. Ann. N. Y. Acad. Sci. 1157, 10–23. https://doi.org/10.1111/j.1749-6632.2009.04534.x.

Graham, A., Shimeld, S.M., 2013. The origin and evolution of the ectodermal placodes. J. Anat. 222 (1), 32–40. https://doi.org/10.1111/j.1469-7580.2012.01506.x.

Lin, F.R., Ferrucci, L., An, Y., et al., 2014. Association of hearing impairment with brain volume changes in older adults. Neuroimage 90, 84–92. https://doi.org/10.1016/j.neuroimage.2013.12.059.

Peelle, J.E., Troiani, V., Grossman, M., Wingfield, A., 2011. Hearing loss in older adults affects neural systems supporting speech comprehension. J. Neurosci. 31 (35), 12638–12643. https://doi.org/10.1523/JNEUROSCI.2559-11.2011.

Hribar, M., Suput, D., Carvalho, A.A., Battelino, S., Vovk, A., 2014. Structural alterations of brain grey and white matter in early deaf adults. Hear. Res. 318, 1–10. https://doi.org/10.1016/j.heares.2014.09.008.

Rönnberg, J., Hygge, S., Keidser, G., Rudner, M., 2014. The effect of functional hearing loss and age on long- and short-term visuospatial memory: evidence from the UK biobank resource. Front. Aging Neurosci. 6, 326. https://doi.org/10.3389/fnagi.2014.00326.

Voermans, N.C., Petersson, K.M., Daudey, L., et al., 2004. Interaction between the human hippocampus and the caudate nucleus during route recognition. Neuron 43 (3), 427–435. https://doi.org/10.1016/j.neuron.2004.07.009.

Nyberg, L., Karalija, N., Salami, A., et al., 2016. Dopamine D2 receptor availability is linked to hippocampal-caudate functional connectivity and episodic memory. Proc. Natl. Acad. Sci. USA 113 (28), 7918–7923. https://doi.org/10.1073/pnas.1606309113.

Schiffer, A.-M., Ahlheim, C., Wurm, M.F., Schubotz, R.I., 2012. Surprised at all the entropy: hippocampal, caudate and midbrain contributions to learning from prediction errors. PLoS ONE 7 (5), e36445. https://doi.org/10.1371/journal.pone.0036445.

Ching, T.Y.C., Dillon, H., Marnane, V., et al., 2013. Outcomes of early- and late-identified children at 3 years of age: findings from a prospective population-based study. Ear Hear. 34 (5), 535–552. https://doi.org/10.1097/AUD.0b013e3182857718.

Gilani, S., Roditi, R., Bhattacharyya, N., 2017. Grade repetition and parents' perception of hearing loss: an analysis of data from children in the United States. Laryngoscope 127 (3), 741–745. https://doi.org/10.1002/lary.26131.

Sarant, J.Z., Harris, D.C., Bennet, L.A., 2015. Academic outcomes for school-aged children with severe-profound hearing loss and early unilateral and bilateral cochlear implants. J. Speech Lang. Hear Res. 58 (3), 1017–1032. https://doi.org/10.1044/2015_JSLHR-H-14-0075.

Ghaziri, J., Tucholka, A., Girard, G., et al., 2018. Subcortical structural connectivity of insular subregions. Sci. Rep. 8 (1), 8596. https://doi.org/10.1038/s41598-018-26995-0.

Ture, U., Yasargil, D.C., Al-Mefty, O., Yasargil, M.G., 1999. Topographic anatomy of the insular region. J. Neurosurg. 90 (4), 720–733. https://doi.org/10.3171/jns.1999.90.4.0720.

X. Wang, Y. Fan, F. Zhao, et al., 2014. Altered regional and circuit resting-state activity associated with unilateral hearing loss, PLoS One. 9(5): e96126–e96126. doi:10.1371/journal.pone.0096126.

Booth, J.R., Wood, L., Lu, D., Houk, J.C., Bitan, T., 2007. The role of the basal ganglia and cerebellum in language processing. Brain Res. 1133 (1), 136–144. https://doi.org/10.1016/j.brainres.2006.11.074.

Husain, F.T., Carpenter-Thompson, J.R., Schmidt, S.A., 2014. The effect of mild-to-moderate hearing loss on auditory and emotion processing networks. Front. Syst. Neurosci. 8, 10. https://doi.org/10.3389/fnsys.2014.00010.